Electron tunneling in tantalum surface layers on niobium

S. T. Ruggiero
Department of Physics, University of Notre Dame, Notre Dame, Indiana 46556

E. K. Track and D. E. Prober
Section of Applied Physics, Yale University, New Haven, Connecticut 06520

G. B. Arnold and M. J. DeWeert
Department of Physics, University of Notre Dame, Notre Dame, Indiana 46556
(Received 10 January 1986)

We have performed electron tunneling measurements on tantalum surface layers on niobium. The tunnel junctions comprise 2000-Å Nb base electrodes with 10—100-Å *in situ*—deposited Ta overlayers, an oxide barrier, and Ag, Pb, or Pb-Bi alloy counterelectrodes. The base electrodes were prepared by ion-beam sputter deposition. The characteristics of these junctions have been studied as a function of Ta-layer thickness. These include the critical current, bound-state energy, phonon structure, and oxide barrier shape. We have compared our results for the product I_cR versus tantalum-layer thickness with an extended version of the Gallagher theory which accounts for both the finite mean free path in the Ta overlayers and suppression of the I_cR product due to strong-coupling effects. Excellent fits to the data yield a value of the intrinsic scattering probability for electrons at the Ta/Nb interface of $r^2=0.01$. This is consistent with the value expected from simple scattering off the potential step created by the difference between the Fermi energies of Ta and Nb. We have found a universal empirical correlation in average barrier height $\bar{\phi}$ and width s in the form $\bar{\phi}=6$ eV/$(s-10$ Å$)$ for measured junctions which holds both for our data and results for available data in the literature for oxide-barrier junctions. The latter are composed of a wide variety of base and counterelectrode materials. These results are discussed in the general context of oxide growth and compared with results for artificial tunnel barriers.

I. INTRODUCTION

There has been considerable interest in tunneling in thin surface layers on Nb because of the success of surface layers in producing very-high-quality junctions on this material. The desire to produce good Nb-based tunnel junctions has been motivated by the desire to study the fundamental properties of Nb and because of its technological importance. Nb has the highest T_c of the elemental superconductors and pure Nb junctions have a robust physical character. Unfortunately, the oxidation of pure Nb typically results in poor tunnel barriers, usually ascribed to suboxide growth. Consequently, the I-V characteristics of pure niobium typically deviate substantially from BCS behavior and may have considerable excess conductance at zero bias and a smearing of the I-V curve in the gap region. In order to improve these characteristics thin overlayers of a second material have been deposited, *in situ,* to cap the Nb surface and form an improved barrier. For example, thin layers of amorphous silicon[1–4] have proven quite successful in forming a good "artificial" barrier. Exceeding these results, however, have been those for thin metal layers. Here it is the natural oxide of the selected surface layer which forms the tunnel barrier. Thin layers of Al (Refs. 5 and 6), Lu (Ref. 7), and Mg, Y, and Er (Ref. 8) have been employed because of their favorable oxidation properties. It has also been shown that refractory metals, Zr (Ref. 9) and Ta (Ref. 10), can be employed with equal success for this purpose. One advantage of the latter materials is the removal of the restriction of lower-temperature deposition of the surface layer. Ta and Zr have also been studied, along with Al layers, because of interest in the structural and microscopic properties of Nb-based multilayer superconductors.[11–14]

The present work involves an investigation of the Nb/Ta system. Here, thin layers of Ta in the range 10—100 Å were deposited on thick (2000 Å) layers of Nb, *in situ,* and oxidized. The junctions were completed with Ag, Pb, and Pb-Bi counterelectrodes. In this paper, we discuss the gap structure, critical current, phonon structure, and barrier shape of these surface-layer tunnel junctions as a function of Ta layer thickness.

II. SAMPLE PREPARATION

Base electrodes were prepared by sequential ion-beam sputtering of Nb and Ta. As previously discussed,[15] this method is capable of producing high-quality refractory-metal films. The deposition chamber employed is a diffusion-pumped, 18-in. Pyrex cylinder equipped with a large-area, internal, liquid-nitrogen-cooled shield. Research grade (99.995%) Xe gas was employed with the ion gun at (uncompensated) ion-gauge pressures of $\sim 1.5\times 10^{-4}$ Torr. Before deposition of the films the niobium target was sputtered for ~ 3 h to getter the chamber. A typical run produced a series of base elec-

trodes each with a different Ta overlayer thickness on a 2000-Å Nb underlayer. This was accomplished by first placing the Nb target beneath the ion beam to deposit Nb on all substrates simultaneously. Next, the Ta target was placed in the beam (within 1 or 2 sec) and Ta was deposited on all substrates for a desired interval. A series of Ta surface thicknesses was obtained by sequentially shuttering substates from the Ta source. In this way a series of samples, each with an identical Nb/Ta interface, was produced.

After deposition the nitrogen shield was allowed sufficient time to warm to room temperature ($\sim\frac{1}{2}$ h). The films were then oxidized either by first bleeding 1–2 Torr of pure oxygen into the chamber and waiting $\sim$10 min or simply breaking vacuum immediately. Next, after a minimum of $\sim$12 min had elapsed, 2000 Å of thermally evaporated Ge was deposited on the samples through a wire mask to protect the base-electrode edges and define a 75-μm-wide line. To create (75 μm$\times$75 μm)-area junctions a second Ge deposition was made at right angles to the first. Otherwise, and more typically, 75 μm$\times$350 μm junctions were made by depositing counterelectrodes through a mechanically slotted mask. The counterelectrode material was Pb, Ag, or a Pb-Bi alloy (29 wt. % Bi).

Initial measurements of the composite-base-electrode junctions typically showed them either to be of high quality (low leakage, sharp gap structure) or to have obvious defects (low-resistance shorts, etc.). Although the detailed mechanisms influencing the junction "mortality" rate are not fully understood, a contributing factor may likely be the characteristics of the air to which the films are exposed[16] (temperature, humidity, etc.) and improved results appeared to be achievable by an initial exposure of the films to pure oxygen. A complete understanding of this behavior may await studies where fabrication takes place entirely *in situ*.

Shown in Fig. 1 is an I-V curve which typifies the results for good junctions with Pb-Bi counterelectrodes. As previously discussed, the application of thin overlayers of Ta, as with Al, can dramatically improve the I-V characteristics of Nb-based junctions. Unless the Ta surface layer is thinner than $\sim$10–20 Å, junctions show sharp gap structure and very low relative conductance at zero bias, typically from 10^{-4} to 10^{-3} of the normal-state conductance. The curves tend to show a small onset of conduction at $eV=\Delta_{\text{Pb-Bi}}$ (1.74 meV at 1.4 K),[17] usually attributed to tunneling from the Pb-Bi electrode into normal material at the base electrode.

Also shown in Fig. 1 is the calculated I-V characteristic for this junction. This I-V was obtained in the standard way by integration over the normalized zero-temperature densities of state for the base electrode and counterelectrode via the formula

$$I(V)=\int_{-\infty}^{\infty} dE\, N_{\text{Nb/Ta}}(E)N_{\text{Pb-Bi}}(E)[f(E)-f(E+eV)]\,, \tag{1}$$

where $f(E)$ is the Fermi function evaluated at the temperature of the experiment. $N_{\text{Pb-Bi}}(E)$ is taken to be a BCS density of states with $\Delta_{\text{Pb-Bi}}=1.74$ meV. $N_{\text{Nb/Ta}}(E)$, shown in Fig. 2, is calculated from the proximity-effect tunneling theory of Wolf and Arnold.[18]

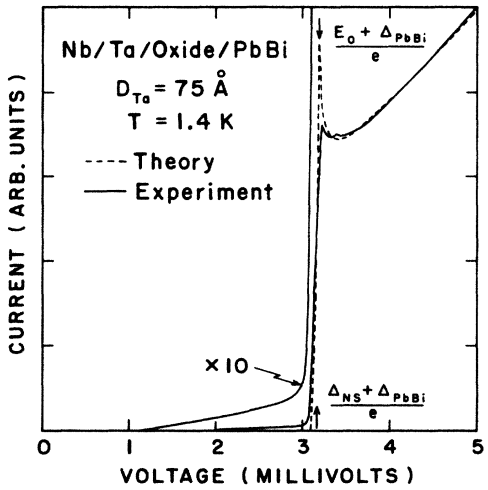

FIG. 1. Shown is the current-voltage (I-V) characteristic of a tunnel junction with a base electrode comprising a 75-A Ta overlayer on 2000 Å of Nb. The junction was air-oxidized and received a Pb-Bi (29 wt.% Bi) counterelectrode. Both the theoretical (dashed line) and experimental (solid line) curves show a sharp peak due to the presence of a quasiparticle bound state in the Ta overlayer. The peak occurs here at a voltage $(E_0+\Delta_{\text{Pb-Bi}})/e$. Here, $\Delta_{\text{Pb-Bi}}=1.74$ meV and $\Delta_{\text{Nb}}=1.51$ meV.

In general, theory and experiment are in excellent accord. In the vicinity of the current rise we see the sharp peak and negative-resistance region associated with the bound state in the Ta surface layer. The experimentally observed attenuation of this peak appears to be due to noise smearing, perhaps in conjunction with dissipative ef-

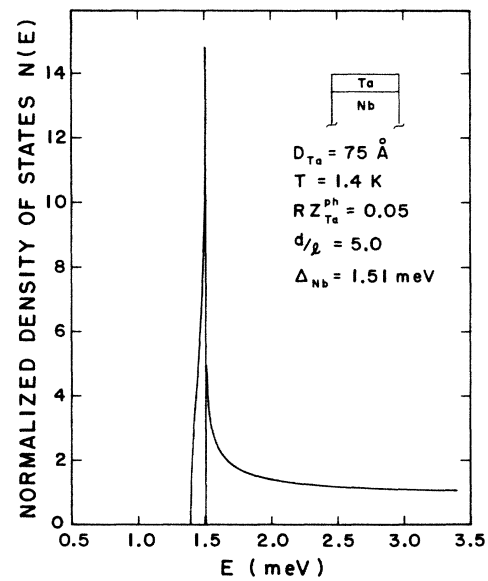

FIG. 2. Proximity density of states of the Ta surface-layer system which was employed to generate the theoretical curve shown in Fig. 1. The first sharp peak represents the quasiparticle bound state in the Ta overlayer occurring at an energy E_0. The dip and rise of $N(E)$ in the vicinity of 1.5 meV is due to a very narrow gap in the density of states between this bound state and the residual BCS peak of the Nb underlayer.

fects due to scattering at the Nb/Ta interface. Also absent from the theory is the previously noted[10] second peak seen in the experimental I-V characteristic just following the bound-state peak. Although, from its energy position ($eV=\Delta_{Nb}+\Delta_{Pb\text{-}Bi}$), this second peak appears to be associated with the Nb density of states, no such structure appears in the theoretical prediction. According to theory, as shown in Fig. 2, the energy difference between the bound-state density of states and the peak of the residual Nb BCS density of states is exceedingly small on the energy scales in question and could not, here, give rise to the observed second peak.

Similar subgap results were observed with Pb counterelectrodes, although without the sharp behavior in the gap region. Also absent with Pb is the especially sharp peak and associated negative-resistance region observed with the Pb-Bi junctions. This behavior appears to be due to an intrinsic gap broadening typical of relatively thick polycrystalline lead films, where the energy gap is a function of crystallographic direction.

III. ENERGY GAP AND CRITICAL CURRENT

Thin surface layers are expected to have a strong influence on superconducting I-V characteristics, especially in the vicinity of the sum gap. If, as in the case of Ta on Nb, the surface layer has a lower T_c than the underlying material, there will be a lower pair potential, denoted Δ_N, in the surface layer compared with that in the underlying bulk material, Δ_S. As discussed by Wolf and Arnold,[18] Andreev scattering of quasiparticles at this N/S boundary will cause at least one bound state to form in the overlayer material at an energy $\Delta_N < E_0 < \Delta_S$.

The existence of this bound state is clearly evident in Fig. 1. Here, it is manifest as a sharp rise peaking at $eV=E_0+\Delta_{Pb\text{-}Bi}$, followed by a negative-resistance region.

As first discussed by Gallagher,[19] the value of E_0 and the product I_cR do not vary in the same way with D_{Ta} in a proximity-effect system. In fact, what is expected—for relatively thin layers—is a slow decrease in E_0 contrasted by an initially very rapid decrease of I_cR.

Plotted in Fig. 3 are the results for E_0 and I_cR as a function of Ta overlayer thickness D_{Ta}. The effective energy gap Δ_{NS}, defined in the usual manner as the point of maximum slope on the rising I-V curve, typically just below the peak at $E_0+\Delta_{Pb\text{-}Bi}$, is plotted in Fig. 1 for reference.

Results for I_cR are also shown in Fig. 3. Although direct chart-recorder traces typically gave a reliable indication of the magnitude of the critical current, I_c, a more accurate means of obtaining this information was to display the I-V curves on an oscilloscope and "tune" for a maximum I_c value by applying a small ($<\pm 1$ G) magnetic field parallel to the junction surface. All measurements were performed in a Dewar which was doubly shielded with μ-metal. It was observed in our studies that the value of the product I_cR (for fixed-area junctions) decreased monotonically with decreasing critical-current density. This result was unexpected as the I_cR product should be a constant of the system. We note, however, that a similar effect has been observed by Smith *et al.*[20] in junctions employing silicon barriers, by Danchi *et al.*[21] in Sn-SnO-Pb junctions, and by Face *et al.*[22] in Ta/Ta_2O_5/Pb-Bi junctions. Halbritter[23] has proposed an explanation for this effect based on resonant tunneling. Danchi *et al.* modeled their observed falloff by assuming an effective noise temperature (presumably extrinsic) of 8 ± 1 K. Therefore, although the participation of extrinsic noise is kept to a minimum by careful shielding and filtering techniques, the effects of noise, in general, perhaps exacerbated by the electronic structure of the barriers themselves, may play a substantial role in the depression of I_cR with junction resistance.

With this in mind we have attempted to remove this effect from our I_cR data. Since one measurement was available on a low-resistance junction ($RA=7.5\times 10^{-4}$ $\Omega\,\text{cm}^2$, $D_{Ta}=25$ Å, $I_cR=1.9$ meV), this datum was plotted as measured (open symbol), while values of I_cR for other values of D_{Ta} were extrapolated to this resistance using available data for I_cR versus R at a particular Ta thickness.

In Fig. 3 the fits to the data (solid lines) are based on an extended version of the Gallagher theory and include the influence of both the finite mean free path in the Ta layers, l, and strong-coupling effects. To compute the latter, the actual phonon densities of state for Nb, Ta, and the Pb-Bi alloy used were employed. The immediate effect of the strong coupling is obvious in the depression of

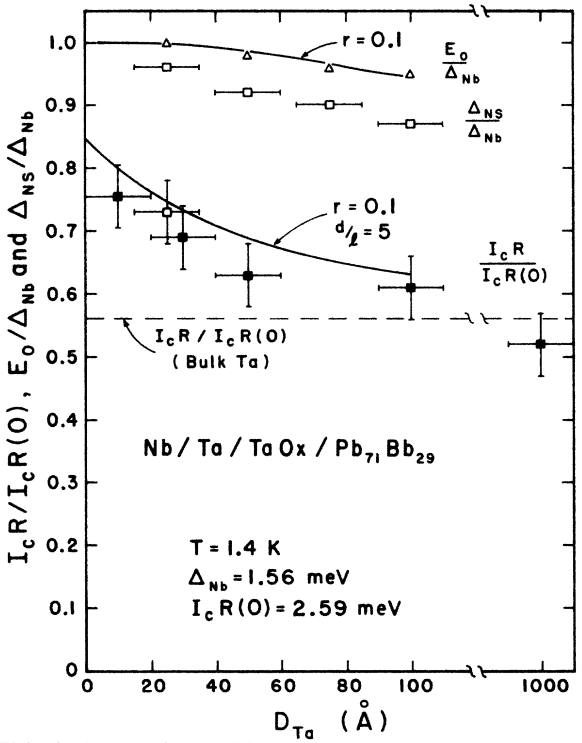

FIG. 3. Normalized critical current, bound-state energy, and measured energy gap are plotted for a series of junctions with increasing Ta overlayer thickness on Nb. Critical currents have been normalized to the value for bulk Nb excluding strong-coupling corrections. Calculations of the critical current include strong-coupling effects from both base-electrode and counterelectrode materials.

the I_cR product in the case where $D_{Ta}=0$ (i.e., for pure Nb) to 84% of its full value in the absence of such effects.

Experimentally, E_0 is very clearly defined and its dependence on D_{Ta} is sensitive to the value of the reflection coefficient, r. Therefore, the data for E_0 were used to establish the magnitude of r as 0.1. With this information (including values of $\Delta_{Pb\text{-}Bi}=1.74$ meV, $\Delta_{Nb}=1.56$ meV, $\Delta_{Ta}=0.72$ meV, and $\xi_{Ta}=130$ Å) and the phonon spectra for bulk Ta, Nb, and Pb-Bi, values of I_cR were generated as a function of D_{Ta}. A fixed value of $d/l=5$ was employed to fit the data as shown, where d is Ta film thickness and l the electronic mean free path, although we note that all values $d/l>1$ produced very similar curves. We see that the theory gives an excellent account of the data, except for a small overall offset which may be due to our extrapolation procedure or may indicate an intrinsic, systematic supression of I_cR.

We note finally that the value of r required to self-consistently fit both the E_0 and I_cR data is close to the value expected on the basis of electron scattering off the small potential step associated with the difference in Fermi energies between Nb and Ta given by[18]

$$r=\left|\frac{v_F(\mathrm{Ta})-v_F(\mathrm{Nb})}{v_F(\mathrm{Ta})+v_F(\mathrm{Nb})}\right| . \tag{2}$$

Average band values of the Fermi velocity $\langle v_F^2\rangle_{E_F}^{1/2}$ of 0.61×10^8 cm/sec for Ta and 0.67×10^8 cm/sec for Nb,[24] yield a value of $r=0.047$. The somewhat higher value as derived from fits to our data ($r=0.1$) may imply some additional scattering due to the presence of interfacial disorder or impurities.

IV. PHONON STRUCTURE

To investigate the nature of the phonon structure of Ta surface layers on Nb, we have also made a qualitative study of second-harmonic data for junctions completed with Ag counterelectrodes. Shown in Fig. 4 is the second-harmonic signal (d^2V/dI^2) versus V for a series of junctions with D_{Ta} ranging from 25 to 100 Å. The data here were normalized by the relative excitation amplitude compared with the normal resistance.

It is clear that for $D_{Ta}\sim75-100$ Å the structure is dominated by and has all the appearance of bulk Ta phonon structure with Nb peaks present but weak in amplitude. For $D_{Ta}=25$ Å the Nb peak structure becomes more like bulk data and, although attenuated, begins to dominate. The crossover thickness seems to be roughly $D_{Ta}\sim50$ Å. It is interesting to note that both the general trend of these data and the value of D_{Ta} where the Ta phonon structure becomes strongly attenuated is similar to the results by Hertel *et al.*[12] In that case the Ta surface layers were first covered (*in situ*) with a thin Al layer to form the tunnel barrier. In addition, and significantly, those Ta surface layers were prepared at elevated temperatures and have much larger (lateral) microcrystalline size. Thus, although Hertel's Ta films were prepared under substantially different conditions than those in this work, the phonon characteristics, at least on the basis discussed, appear similar.

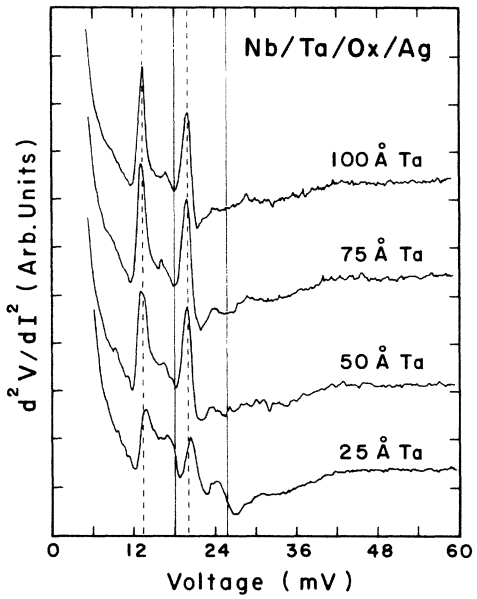

FIG. 4. Second-harmonic signal (d^2V/dI^2) versus voltage for a series of Ta surface-layer junctions. Indicated are the relative positions of the Ta (dashed lines) and Nb (solid lines) transverse- and longitudinal-acoustic-phonon energies.

V. BARRIER SHAPE

Important to the electrical characteristics of tunnel junctions is the detailed nature of their tunnel barriers. The simplest means of describing a barrier is to assume that tunneling occurs through a trapezoidal WKB barrier of a given width, height, and asymmetry. A simplified expression for the current-voltage relation in this case was originally presented by Simmons,[25] and later extended by Chow.[26] Rowell and Brinkman *et al.*[27] have described a simple means of extracting barrier parameters from the Simmons model.

We note that this model represents an idealized picture of what in reality may be a rather complicated tunneling process. For example, it has become increasingly clear that secondary tunnel channels may exist in nonuniform oxide layers. It has been pointed out by Gundlach *et al.*[28] that under these circumstances a measure of the effective barrier height can be obtained from a plot of the logarithmic derivative of the conductance, $\hat{g}=d\ [\ln(I/V)]/dV$, versus voltage, which displays a peak at a voltage slightly higher than the barrier height. Magerlein[29] has noted the ability of this method to resolve potential ambiguities in the evaluation of barrier heights.

However, in order to employ this method, junctions must be biased to voltages which in the case of relatively-low-resistance junctions may cause excessive self-heating or other deleterious, nonreversable effects. Although this has precluded a general analysis of the barrier properties of our Ta surface-layer junctions by this method, we have noted—for our junctions—that $\hat{g}$ does display a peak at a bias of 30—50 meV. This may be due to the onset of resonant tunneling[30] via states in the oxide lying within this voltage range below the Fermi level of the base elec-

trode. We did not, however, observe any additional peaks up to the maximum voltage to which the data were taken (0.6 V). In the context of the resonant-tunneling model this would tend to indicate the absence of a low-barrier channel of the type attributed to niobium-oxide barriers.

With these issues in mind, we have employed the Simmons model as a basic, parametric tool for studying trends in the effective WKB barrier shape of our junctions. We will also discuss comparative trends in other published data acquired in the same fashion. In our analyses we have typically employed differential conductance data in the range -500 to 500 meV.

In the context of this trapezoidal barrier model, typical air-oxidized Nb junctions have rectangular, low (~ 0.3 eV), and broad (~ 25 Å) barriers. Such junctions also show less than ideal tunneling characteristics. Although there is no intrinsic reason why such a barrier should necessarily produce poorer I-V curves, and (as discussed above) the actual barrier is in reality perhaps not so simply represented, such a barrier—at least in the case of niobium—is associated with poorer I-V's. Indeed, the presence of multiple tunnel channels may well be the cause for both the lowering of the effective barrier height of these junctions and other associated anomalies.

In our work, it has been found that when sufficiently thick surface layers of tantalum are applied to the surface of niobium (and, as will be discussed, oxidation is not excessive) our junctions display both the high and narrow (and asymmetric) barrier shape and sharp I-V characteristics associated with high-quality junctions formed on pure Ta.[22,31] It is particularly interesting to note, in this regard, that recent studies of specially prepared pure Nb junctions by Celaschi *et al.*[32] have resulted in the formation of high (0.7 eV), narrow (20 Å) barriers which show high-quality I-V characteristics. It is clear, therefore, that when the effective barrier of a Nb-based junction is made higher, either by the application of a thin surface layer or by the special preparation of pure Nb, highly improved tunneling characteristics are the result.

Shown in Fig. 5 are the results for the average barrier height $\bar{\phi}$ and width s of our Nb/Ta junctions and for pure Ta (Ref. 22) and Nb (Refs. 32–34). These parameters were obtained from the Simmons model as previously discussed. It is seen that barrier shape can vary considerably—from the high (>1 eV), narrow (<20 Å) barriers associated with pure Ta to the low (~ 0.3 eV), broad (~ 30 Å) shape more common to pure Nb. What we have found is that for sufficiently thick Ta surface layers, $D_{\mathrm{Ta}} > 20$ Å, the initial barrier shape is generally high ($\bar{\phi} \sim 0.8$ eV), narrow ($s < 20$ Å), and independent of D_{Ta}. Also, as depicted in the inset of this figure for a series of junctions with $D_{\mathrm{Ta}} = 100$ Å and also observed with Al overlayers (Ref. 33), and junctions of pure Ta (Ref. 35), higher barrier asymmetry was associated with greater average barrier height. We also note that, again as with Al, below some surface-layer thickness, in the case of Ta ~ 10–20 Å, symmetric, low, and wide barriers—and impaired junction characteristics—typically associated with pure Nb were observed. In Table I we have listed the available parameters for junctions studied.

These data for $D_{\mathrm{Ta}} = 100$ Å, and those for Ta surface-layer junctions having a wide range of Ta layer thicknesses, tend to behave according to the general rule that as oxidation proceeds barrier height decreases and barrier width increases. Thus, for a given surface-layer thickness one starts at some point on the $\bar{\phi}$-versus-s curve (Fig. 5) and proceeds down the curve or parallel to it as s increases. We note that as long as D_{Ta} is greater than ~ 20 Å the overlayer thickness does not appear to strongly influence initial $\bar{\phi}$ and s values, which may depend more critically on initial oxidation conditions. In contrast, junctions with thinner Ta layers (<10–20 Å) tend always to have lower broad barriers.

To obtain a broader perspective on this behavior, data for a variety of systems available in the literature, which span a large range of $\bar{\phi}$, have been plotted in Fig. 6. Here we have included results for pure Al (Refs. 27 and 36) Ta (Ref. 22), and Nb (Refs. 32–34), and data for overlayers of Al (Ref. 33) and Ta (this work) on Nb where a variety of counterelectrodes was employed. As seen in the preceding figure, both within a given system and for the data in general there is a monotonic decrease in the aver-

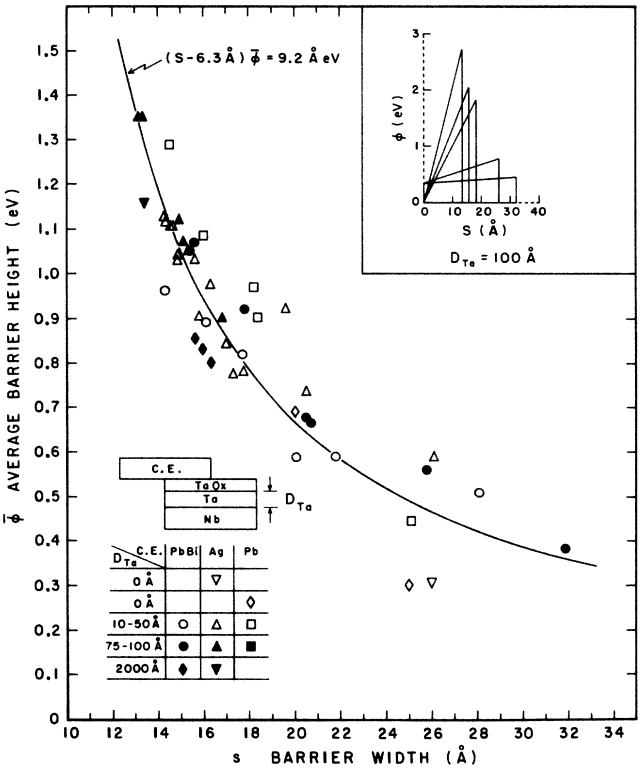

FIG. 5. The main portion of this figure shows the average WKB barrier height versus barrier width for tunnel junctions with base electrodes of pure Ta (2000 Å Ta), pure Nb, and various Ta overlayer thicknesses on Nb. The data include results for various counterelectrodes (C.E.) including Pb-Bi, Ag, and Pb. The solid line shows an empirical fit to the data. Shown in the inset are the barrier shapes of a series of our junctions all with base electrodes comprising 100 Å Ta on 2000 Å Nb. This series of data illustrates the trend that as oxidation proceeds, the barriers go from being high, narrow, and asymmetric to low, broad, and symmetric. (▽, Ref. 33; ◇, Ref. 32; ○, △, □ ●, ▲, and ■, this work; ◆ and ▼, Ref. 22).

age barrier height $\bar{\phi}$ with barrier width s. In this case, this broader range of data implies a best empirical fit of $\bar{\phi}(s-10.4\ \text{Å})\sim 6\ \text{eV Å}$.

The observed decrease in the barrier height with width of natural oxide barriers may involve a variety of participating phenomena. For niobium-like oxide barriers Halbritter has suggested an explanation based on the existence of a multicomponent oxide layer. In this model, the effective barrier height decreases due to the opening of parallel tunnel channels of low effective barrier height as oxidation proceeds.[30,37]

Another approach is to consider oxide growth to be a self-terminating process. As first formulated by Cabrerra and Mott[38] and later extended by Fromhold,[39] the growth of an oxide on a metal surface will essentially terminate when the effective barrier thickness becomes too large to

TABLE I. Parameters of Ta surface-layer tunnel junctions.

Sample	Counter-electrode	Ta thickness (Å)	Area (μm×μm)	Resistance (Ω)	Δ_{NS} (meV)	I_c (μA)	I_cR (mV)	Barrier width s (Å)	Average barrier height $\bar{\phi}$ (eV)	Barrier asymmetry[a] $\Delta\phi$ (eV)
1	Pb-Bi	100	75×350	18	3.04	60	1.08	15.36	1.05	2.00
2	Pb-Bi	100	75×350	26	3.1	30	0.78	15.6	1.07	2.14
3	Pb-Bi	100	75×350	86	3.1	0.39	0.034	17.81	0.92	(1.87)
4	Pb-Bi	75	75×350	96.6	3.14			20.6	0.678	0.611
5	Pb-Bi	75	75×350	94.7	3.14	0.6	0.057	20.7	0.666	0.545
6	Pb-Bi	75	75×350	100	3.14	0.5	0.05	20.5	0.678	0.521
7	Pb-Bi	50	75×350	21.7	3.1	46	1.0	20.1	0.587	0.296
8	Pb-Bi	50	75×350	19.5	3.18	6.3	1.23			
9	Pb-Bi	25	75×350	91.3	3.24	0.18	.016	21.77	0.59	0.411
10	Pb-Bi	25	75×350	11.68	3.24	127	1.48	16.13	0.89	1.09
11	Pb-Bi	25	75×350	2.87	3.24	660	1.89	14.27	0.963	1.12
12	Pb-Bi	0	75×350	310000	3.25					
13	Pb-Bi	0	75×350	550000	3.25					
14	Ag	100	75×350	55				16.8	0.998	(2.07)
15	Ag	100	75×350	8.7				13.2	1.35	(2.99)
16	Ag	100	75×350	9.3				13.24	1.351	3.13
17	Ag	75	75×350	3.73						
18	Ag	75	75×350	17				14.9	1.12	2.06
19	Ag	75	75×350	15				15.1	1.069	1.96
20	Ag	50	75×350	11.76						
21	Ag	50	75×350	8.7				14.84	1.033	1.40
22	Ag	50	75×350	9.5				15.8	0.903	1.29
23	Ag	25	75×350	10.75				14.58	1.106	2.04
24	Ag	25	75×350	8.33				14.32	1.113	1.99
25	Ag	25	75×350	9.46				14.84	1.04	1.67
26	Pb	40	75×350	121.8	2.68			18.36	.897	1.48
27	Pb	40	75×350	45.4	2.81			15.96	1.086	2.26
28	Pb	40	75×350	30.6				14.49	1.288	3.23
29	Pb	20	75×350	151.9	2.7					
30	Pb	20	75×350	202.4	2.83			18.21	0.969	0.716
31	Pb	20	75×350	310						
32	Pb	10	75×350	110.2	2.78					
33	Pb	10	75×350	83.3	2.87			25.13	0.395	0.304
34	Pb	10	75×350	49.8						
35	Pb	0	75×75	34500	2.88					
36	Ag	40	75×350	16.53				15.33	1.05	1.84
37	Ag	40	75×350	19.31				15.6	1.03	1.90
38	Ag	40	75×350	27.1				16.3	0.975	1.79
39	Ag	30	75×350	8.56				14.27	1.125	1.89
40	Ag	30	75×350	11.24				14.63	1.105	2.01
41	Ag	20	75×350	21.7				17.74	0.779	0.903
42	Ag	20	75×350	18.35				16.98	0.842	0.982
43	Ag	10	75×350	14				17.3	0.773	(1.72)
44	Ag	0	75×75							

[a]Barrier asymmetries in excess of $2\bar{\phi}$ (indicating a breakdown of the trapezoidal barrier model) have been listed in parentheses.

permit sufficient electron tunnel current to balance the ionic transport across the oxide during the growth process. This simply implies that if a growing oxide in question has an intrinsically larger barrier height, it will terminate its free growth (or experience a sharp reduction in growth rate) at a smaller thickness.

The point at which the growth "terminates" can be expressed as the point at which the electron current density just equals the ionic current density through the oxide. Therefore if

$$J_e=\frac{6.2\times10^{10}}{L^2}[\phi_1 e^{-1.025L(2\phi_1)^{1/2}} -(\phi_1-V_m)e^{-1.025(2\phi_1-V_m)^{1/2}}],$$

where

$$\phi_1=\bar{\phi}+\tfrac{1}{2}V_m$$

and

$$J_i=(9.63\times10^{-4})(\bar{A}Z/v)\sinh(\bar{L}/L),$$

then the self-limiting oxide thickness L is defined through the relation $J_e(L)=J_i(L)$.[38–40] Here, V_m is the Mott potential, $\bar{A}$ the oxide growth rate, $\bar{L}$ a normalized oxide thickness, Z the charge of the diffusing metal ion, and v the molar volume of the growing oxide.

Using measured values for these parameters for carefully controlled oxide growth on metals, within the stated experimental uncertainties,[41] we have reproduced the Celaschi[32] niobium datum exhibiting a barrier height of 0.7 eV. Here we have taken the Mott potential V_m as $0.2\bar{\phi}=-0.14$ eV. Keeping parameters fixed (including V_m), and varying the effective barrier height, the rest of the barrier-height—versus—width curve has been generated and appears in Fig. 6 as the dotted line. As previously discussed, one can also fit these data by assuming that V_m varies as $0.2\bar{\phi}$ over the entire curve, producing a similar fit to the data. This reflects the expected result that a higher oxidation potential (and thus a higher Mott potential) is typically associated with oxides exhibiting larger barrier heights, such as Al_2O_3. In any case, the theory tends to reproduce the general trend of the oxide-barrier data.

This approach cannot, however, answer the question of why for a given material, such as aluminum or niobium, oxides should grow which exhibit effective barrier heights of differing magnitude. The theory simply tells us that if an oxide grows with a lower barrier height, its thickness will terminate at a larger value. The explanation for this may well lie in the detailed microscopic structure of the oxide itself, the effective barrier height it ultimately manifests being determined by a perhaps highly complex physical and electronic structure dependent, in turn, on oxide-growth conditions.

An even more encompassing perspective of the behavior of tunnel barriers has been obtained by including on this plot the results for so-called "artificial barriers," plotted with larger symbols. These barriers are not natural oxide layers grown on the base-electrode layer of a junction, but rather prepared by the separate deposition of a tunnel barrier on the base-electrode surface. Included here are results for electron-beam-[42] and sputter-deposited[43] aluminum oxide and silicon.[4] These data tend to both lie in the general vicinity of the natural oxide data and tend, to some extent, to follow a similar trend of average barrier height with width. This is especially evident for the silicon barriers which have particularly low effective heights. In light of these data we have also plotted on this figure (as solid lines) curves of constant current density. Thus for junctions with constant areas, these curves would translate to those for constant junction resistance. In this context, it is clear that the data overall are denser in the vicinity of $0.1<J<10$ A/cm^2. This suggests that there may be a statistical predisposition for data to be found in this region. That is, if one moves sufficiently off this curve, junctions would exhibit current densities beginning to become prohibitively high or low enough to completely preclude measurement or prohibit measurements to sufficiently high voltages to gather information on barrier shape.

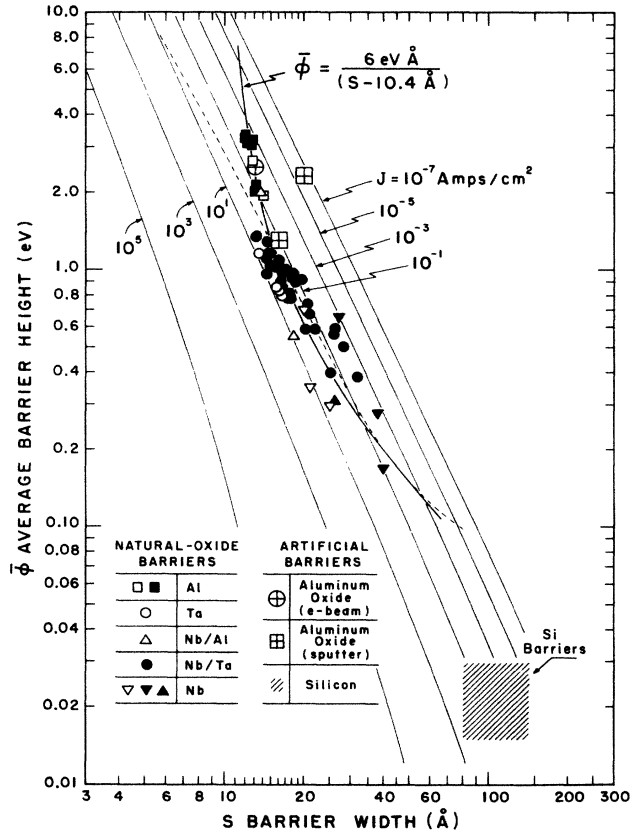

FIG. 6. Shown is the average barrier height versus width for junctions composed of a wide variety of base-electrode and counterelectrode materials. The solid line is an empirical fit to the data. Also shown (dashed line) is the theoretical prediction of the Fromhold—Mott-Cabrera theory which describes self-limiting oxide growth on free metal surfaces. Curves of constant current density for a fixed bias voltage of 10 meV are shown as solid lines. Data for artificial barriers composed of electron-beam- (Ref. 42) and sputter-deposited aluminum oxide (Ref. 43) and for Si (Ref. 4) are also shown for comparison (□ and ■, Refs. 27 and 36; △, Ref. 33; ●, this work; ○, Ref. 22; ▽, ▼, and ▲, Refs. 32—34).

However, although both sets of data (natural and "artificial") may therefore naturally lie in the same general region of current density, their individual trends of barrier height with width may be different. As previously discussed,[10] a series of oxide barriers, produced under similar conditions, will show a decrease in barrier height for barriers of somewhat greater thickness. This may not be true for artificial barriers. Preliminary results for aluminum-oxide barriers[43] show a greater effective barrier height for thicker barriers, even though—again—these data lie in the general vicinity of the oxide-barrier results.

Therefore we conclude that because of the restrictions imposed by actual measurements of junctions and the strong dependence of critical current density with effective barrier parameters, data for effective barrier height versus width will necessarily show a general trend of decreasing barrier height with width. However, for a given class of systems, this may not be true on a local scale, depending on the particular mechanism(s) governing barrier parameters.

VI. CONCLUSIONS

We have found that thin Ta surface layers on Nb can be reliably used to produce tunnel junctions with nearly ideal characteristics. The detailed shape of the I-V curve of a Nb/Ta junction, including a sharp bound-state peak, has, for the first time, been accurately reproduced by the proximity-effect tunneling theory.

Both the critical current and bound-state energy position of the junctions have been studied as a function of Ta surface-layer thickness. Calculations of the critical current were performed including strong-coupling corrections from both base-electrode and counterelectrode metals. Self-consistent fits to the bound-state energy E_0 and product I_cR versus D_{Ta} are in accord with the proximity-effect theory and give a value for the electron reflection probability at the Nb/Ta interface of $r^2=0.01$. This value is consistent with the simple model which assumes that a major fraction of this interfacial scattering is due to the potential step created by the Fermi-level difference between Nb and Ta.

We have studied the behavior of the phonon structure of Ta surface layers on Nb as a function of Ta thickness. It is seen that the Ta phonon structure dominates the observed spectra until $D_{\mathrm{Ta}} \lesssim 50$ Å and that, by all indications, there is no mixing but a simple superposition of these spectra.

Finally we have shown that studies of both pure and surface-layer junctions reveal a general trend in barrier shape and width. The systematic decrease in barrier height with increasing width, although perhaps linked to those processes governing oxide growth on free metal surfaces, may have its origins in the detailed electronic structure of the barriers themselves and be amplified by basic limitations imposed by data acquisition.

ACKNOWLEDGMENTS

We gratefully acknowledge many useful conversations with M. R. Beasley, M. Gurvitch, J. M. Rowell, D. A. Rudman and W. J. Tomasch and others during the course of this work. We also acknowledge support by the National Science Foundation (NSF) Grant No. ECS-83-05000, U. S. Office of Naval Research (ONR) Contract No. N00014-80-C-0855 at Yale University, and NSF Grant No. ECS-85-06823 at the University of Notre Dame.

[1]D. F. Moore, R. B. Zubeck, J. M. Rowell, and M. R. Beasley, Phys. Rev. B **20**, 2721 (1979).

[2]D. A. Rudman and M. R. Beasley, Appl. Phys. Lett. **36**, 1010 (1980).

[3]H. Kroger, L. N. Smith, and D. W. Jillie, Appl. Phys. Lett. **39**, 280 (1981).

[4]R. Meservey, P. M. Tedrow, and J. S. Brooks, J. Appl. Phys. **53**, 1563 (1982).

[5]E. L. Wolf, J. Zasadzinski, J. W. Osmun, and G. B. Arnold, J. Low Temp. Phys. **40**, 19 (1980).

[6]M. Gurvitch, M. A. Washington, and H. A. Huggins, Appl. Phys. Lett. **42**, 472 (1983).

[7]C. P. Umbach, A. M. Goldman, and L. E. Toth, Appl. Phys. Lett. **40**, 81 (1982).

[8]J. Kwo, G. K. Wertheim, M. Gurvitch, and D. N. E. Buchanan, IEEE Trans. Magn. **MAG-19**, 795 (1983).

[9]S. Celaschi, T. H. Geballe, and W. Lowe, in Proceedings of the Material Research Society, 1982, p. 241 (unpublished); S. Celaschi, R. Hammond, T. H. Geballe, W. P. Lowe, and A. Green, Bull. Am. Phys. Soc. **28**, 423 (1983).

[10]S. T. Ruggiero, D. W. Face, and D. E. Prober, IEEE Trans. Magn. **MAG-19**, 960 (1983); S. T. Ruggiero, G. B. Arnold, E. Track and D. E. Prober, in *Proceedings of the 17th International Conference on Low-Temperature Physics,* edited by U. Eckern, A. Schmid, W. Weber and H. Wühl (North-Holland, New York, 1984), p. 847; IEEE Trans Magn. **MAG-21**, (850) 1985.

[11]J. Geerk, M. Gurvitch, D. B. McWhan, and J. M. Rowell, Physica, **109&110B**, 1775 (1982); D. B. McWhan, M. Gurvitch, J. M. Rowell, and L. R. Walker, J. Appl. Phys. **54**, 3886 (1983).

[12]G. Hertel, D. B. McWhan, and J. M. Rowell, in *Superconductivity in d- and f-Band Metals* (Kernforschungszentrum Karlsruhe, Karlsruhe, 1982), p. 299.

[13]W. P. Lowe, J. Celaschi, and T. H. Geballe, Bull. Am. Phys. Soc. **28**, 508 (1983).

[14]Subject reviewed by S. T. Ruggiero and M. R. Beasley, in *Synthetic Modulated Structures,* edited by L. L. Chang and B. C. Giessen (Academic, New York, 1985).

[15]D. W. Face, S. T. Ruggiero, and D. E. Prober, J. Vac. Sci. Technol. A **1**, 326 (1983).

[16]M. Gurvitch (private communication).

[17]R. C. Dynes and J. M. Rowell, Phys. Rev. B **11**, 1884 (1975).

[18]E. L. Wolf and G. B. Arnold, Phys. Rep. **91**, 31 (1982).

[19]W. J. Gallagher, in *Proceedings of the 16th International Conference on Low Temperature Physics* [Physica **108B**, 825 (1981)]; W. J. Gallagher, Phys. Rev. B **22**, 1233 (1980).
[20]L. N. Smith, J. B. Thaxter, D. W. Jillie, and H. Kroger, IEEE Trans. Magn. **MAG-18**, 1571 (1982).
[21]W. C. Danchi, J. B. Hansen, M. Octavio, F. Habbal, and M. Tinkham, Phys. Rev. B **30**, 2503 (1984).
[22]D. W. Face *et al.* (unpublished).
[23]J. Halbritter, IEEE Trans. Magn. **MAG-19**, 799 (1983).
[24]B. Chakraborty, W. E. Pickett, and P. B. Allen, Phys. Rev. B **14**, 3227 (1976).
[25]J. G. Simmons, in *Tunneling Phenomena in Solids*, edited by E. Burstein and S. Lundquist (Plenum, New York, 1969).
[26]C. K. Chow, J. Appl. Phys. **36**, 559 (1965).
[27]J. M. Rowell, in *Tunneling Phenomena in Solids*, Ref. 25; W. F. Brinkman, R. C. Dynes, and J. M. Rowell, J. Appl. Phys. **41**, 1915 (1970).
[28]K. H. Gundlach, G. Faraci, G. Giaquinta, and N. A. Mancini, Phys. Lett. **43A**, 27 (1973).
[29]J. H. Magerlein, J. Appl. Phys. **55**, 4027 (1984).
[30]J. Halbritter, J. Appl. Phys. **58**, 1320 (1985), and references therein.
[31]E. G. Spencer and J. M. Rowell, IEEE Trans. Magn. **MAG-17**, 322 (1981).
[32]S. Celaschi, T. H. Geballe, and W. P. Lowe, Appl. Phys. Lett. **43**, 794 (1983).
[33]J. M. Rowell, M. Gurvitch, and J. Geerk, Phys. Rev. B **24**, 2278 (1981).
[34]D. G. Walmsley, E. L. Wolf, and J. W. Osmun, Thin Solid Films **62**, 61 (1979).
[35]A. Hahn, M. Brunner, and H. Ekrut, Thin Solid Films **102**, 221 (1983).
[36]M. A. Ocampo, J. L. Heiras, and T. A. Will, J. Appl. Phys. **53**, 3698 (1982).
[37]J. Halbritter (unpublished).
[38]N. Cabrera and N. F. Mott, Rep. Prog. Phys. **12**, 163 (1949).
[39]See A. T. Fromhold, Jr., *Theory of Metal Oxidation* (North-Holland, New York, 1976) Vol. 1.
[40]A. T. Fromhold, Jr. and E. L. Cook, Phys. Rev. **158**, 600 (1967); M. J. Dingham, W. R. Fawcett, and H. Bohni, J. Electrochem. Soc. **113**, 656 (1982).
[41]M. Grundner and J. Halbritter, Surf. Sci. **136**, 144 (1984).
[42]S. J. S. Moodera, R. Meservey, and P. M. Tedrow, Appl. Phys. Lett. **41**, 488 (1982).
[43]J. B. Barner and S. T. Ruggiero (unpublished).